Scripta METALLURGICA et MATERIALIA
Vol. 26, pp. 19-24, 1992
Printed in the U.S.A.
Pergamon Press plc

SELECTIVE PARTICLE DRAG DURING PRIMARY RECRYSTALLIZATION OF Fe-Cr ALLOYS

D. Raabe, K. Lücke
Institut für Metallkunde und Metallphysik
RWTH Aachen, W-5100 Aachen, Germany

(Received September 4, 1991)
(Revised October 14, 1991)

Introduction

The cold rolling texture of bcc steels usually shows a strong <110> fibre parallel rolling direction (α-fibre) containing the orientations {001}<110> -{112}<110> and {111}<110>, and a <111> fibre parallel normal direction (γ-fibre) with {111}<110> and {111}<112> (6), (Fig.1).
During cold rolling typically a strong α-fibre, with a maximum at {001}<110> to {112}<110> develops, which, after primary recrystallization is shifted to {111}<112>. This maximum normally is explained by a combination of oriented nucleation and oriented growth of large angle grain boundaries (6,15,16). The influence of nucleation in the development of {111}<112> is based on high dislocation density, high Taylor factor and influence of former grain boundaries in {111}<uvw> regions (8,6,2,15). In the case of annealing, an oriented nucleation can take place.
The theory of oriented growth describes the second important mechanism in the formation of recrystallization textures (6,4,7). The rotation relationship of ≈35°<110> between the strong cold rolling component {112}<110> and the recrystallization component {111}<112> is quite close to the ideal coincidence rotation of 27°<110> which is well known for a high mobility and leads to a very quick growth of {111}<112> oriented nuclei into {112}<110> regions. The weak point in this argumentation is the deviation of 7° from the ideal coincidence.
The subjects of this investigation, however, are Fe-Cr alloys in which the true 27°<110> rotation relationship was found. An orientation {557}<583>, which had not yet been discussed properly in texture analysis, seemed to grow into the strong {112}<110> component and became the absolute maximum in the recrystallization texture.
As the reason for this oriented growth, an energy selective particle drag is suggested.

Description of bcc Textures

Textures of bcc metals are investigated by measuring pole figures according to Bragg's law. A quantitative analysis of pole figures taken from polycrystals leads to a high degree of ambiguity because of the superposition of the considered types of poles. To receive a less ambiguous description of textures, the orientation distribution function (ODF) has to be calculated from four different pole figures. An orientation then can be represented by the three eulerian angles φ_1, Φ and φ_2. In the submitted investigation the ODF is calculated from four different pole figures (110, 200, 112, 103) by the series expansion method (ℓ_{max}=22) and is represented in the reduced eulerian space (5). The information of this space can be compressed into certain orientation fibres where the orientation density is shown versus one eulerian angle whilst in the case of α-, γ- and η-fibre, the other angles remain constant (6),(Fig.1):

(1)	α-fibre	<110>	RD : {001}<110>, {112}<110>, {111}<110>
(2)	γ-fibre	{111}	ND : {111}<110>, {111}<112>
(3)	η-fibre	<100>	RD : {001}<100>, {011}<100>
(4)	β-fibre	≈{111}	ND no static fibre, φ_1 is abscissa, but Φ and φ_2 can vary according to maximum.

0036-9748/92 $5.00 + .00

Experimental and Results

To investigate the influence of particles on the mobility of coincidence boundaries, two Fe-Cr alloys containing stable microcarbonitrides (samples B and C) and one alloy without stable particles (samples A) were analyzed (Table 1).
The particle size distribution was measured by TEM.
All three alloys were cold rolled to 70%, 80% and 90%, and finally annealed for 200 seconds at 960°C. All processing steps were metallographically analyzed with a scanning electron microscope and the ODFs were determined by measuring four incomplete pole figures in the back reflection mode with $MoK_{\alpha 1}$-rays to serve as input for the serious expansion method (5).
Since s is the distance between layer and sample center divided by the half thickness, all samples were measured at s=0.0 (center), s=0.4, s=0.8 and s=1.0 (surface).
In Fig.2 the texture of the starting material in the hot rolled and annealed state is shown for the Nb-alloyed steel. The texture is very inhomogeneous through the sample thickness. In the sample center (S=0) a typical "cold rolling" texture with a {112}<110> peak has developed which is due to flat and strongly deformed grains which did not recrystallize during hot rolling. Closer to the surface (S>0.7) a typical surface shear texture with a maximum at {011}<100> has developed due to the large grains, the strong pass sequence, and the friction between band surface and rolls (6,7).
In Fig.3a the cold rolling texture of alloy A is shown after 80% and 90% in the sample center. With increasing rolling degree, strong maxima at {001}<110> and {112}<110> on the α-fibre and a weaker peak at {111}<110> on γ-fibre is built up. Figure 3b shows the well-known corresponding recrystallization textures with a strong peak at ≈{111}<112>.
Figure 4a shows the rolling texture, development of alloy C with Nb-carbonitrides after 70%, 80% and 90% in the center of the sample. Again a strong {112}<110> becomes the maximum of the cold rolling texture as also seen in Fig.3a. The recrystallization texture, however, reveals a totally unusual peak at ≈{557}<583> (17,6). Also alloy B, which is a Ti-microalloyed steel, shows a typical strong {112}<110> maximum in the rolling texture (Fig.5a) and after recrystallization this unusual peak at {557}<583>. In Fig.5b a clear shifting from {111}<112> (70%) to {557}<583> (90%) is seen.
In Fig.6a the weak rolling texture of alloy B due to the weak starting texture at the surface is shown. Because of the low {112}<110> component, there is no {557}<583> but only {111}<112> to be found in the recrystallization texture (Fig.6b).
In Fig.7a the texture development is shown through the sample thickness after 90% cold rolling, which reveals a strong {112}<110> in the center and a weak {001}<110> and {112}<110> at the surface. The inhomogeneity of the cold rolled sample is due to the inhomogeneity of the starting material (Fig.2) (6,7). In Fig.7b just this center texture, with a {112}<110> peak, shows {557}<583> after primary recrystallization, whereas the weaker surface texture leads to a {111}<112> recrystallization peak.

Discussion

The "classical" recrystallization peak in Fig. 3b at {111}<112> can be explained by a combination of oriented nucleation of {111}<112> grains in {111}<110> regions and a good growth relationship 30° around <111> (2,15), whereas the textures shown in Figs.4,5,6 and 7 have to be discussed in detail:
All measurements reveal two main tendencies:
(1) A strong {112}<110> cold rolling texture leads to a {557}<583> maximum in the recrystallization texture in alloys with stable microcarbides. This relationship can be described by a 27°<110> rotation which is due to a Σ19a coincidence boundary in bcc.
(2) A strong {112}<110> rolling component in an alloy without stable microcarbides leads to a {111}<112> recrystallization peak.
This behaviour can be explained by selective particle drag. According to Ze-

ner and Gladman (10,13) the retarding force is

$$F_P = \frac{6\gamma(g)\,f}{\pi r}$$

where f is the dispersed volume fraction of stable microcarbonitrides, r the average particle radius and $\gamma(g)$ the grain boundary energy which is a function of 8 parameters (Table 2),(1,3,9). Ignoring the minor importance of the translation vector and spatial position, the grain boundary energy remains dependent of 3 misorientation parameters (e.g. eulerian angles or axis and rotation angle) with the rotational matrix g (Fig.8). That means that the particle drag during primary recrystallization F_P is proportional to the energy of the grain boundary which crosses a carbonitride $\gamma(g)$. This explains the selective effect of F_P.
On the other hand, the driving force for primary recrystallization is given by $F_R \simeq 1/2Gb^2(\Delta\rho)$ where G is the shear modulus, b the Burgers vector and ρ the dislocation density (Table 2).
Fe-Cr steels show a very strong recovery before recrystallization which can be seen in Figs.9a and 9b. This lowers the dislocation density and the driving force of recrystallization. The kinetics of recovery can be described by a differential equation of the first order: $d\rho/dt = -k\cdot\rho$ which leads to $\Delta(\ln\rho) = -k(\Delta t)$, so that the lowered dislocation density at the beginning of primary recrystallization can be calculated. Comparing the approximate values for F_P and F_R which are given in Table 2, it is obvious that the 27°<110> low energy boundary is not very much influenced ($F_R \geqslant F_P(\gamma_{min})$), whereas non special boundaries can be hindered by particles ($F_R > F_P(\gamma_{max})$). Applying the minimum particle sizes, the drag forces can be estimated even much higher, so that they reach the values of the driving forces. Additional to the decrease of the effective driving force of primary recrystallization by particle drag, the activation energy of the grain boundary mobility is much higher in the case of non-special grain boundaries, hence the velocity, which is determined by driving force minus drag force and mobility, can be strongly lowered.

Conclusions

In the submitted paper a new important textural component {557}<583> has been found which develops during primary recrystallization of Fe-Cr alloys with stable particles.
This new orientation was explained by oriented growth, which was caused by grain boundary energy selective particle drag.

References

1. Y.S. Avramov, A.G. Gvozdev, phys. of met., 36,2,No.5, p.198 (1973)
2. W.B. Hutchinson, ICOTOM 9, ed. by J.S. Kallend and G. Gottstein (1988)
3. W. Bollmann, A.J. Perry, Phil. Mag. 20, p.33 (1969)
4. G. Ibe, K. Lücke, Arch. Eisenhüttenwesen, 39 (1968), 693
5. H.J. Bunge, Texture analysis in mat. science, Butterworth, London, 1982
6. M. Hölscher, D. Raabe, K. Lücke, steel research, spec. edition, 1991
7. M. Hölscher, Ph.D. Thesis, 1987
8. U.v. Schlippenbach, Ph.D. Thesis, 1987
9. S.S. Hansen, J.B. Vander Sande, Met. Trans., Vol.11A, 3,80, p.387 (1980)
10. C. Zener, Trans. AIME, Vol.175, p.15 (1949)
11. W. Mao, Ph.D. Thesis, 1988
12. M.J. Ashby, R. Ebeling, Trans. TMS-AIME, 1966, vol.236, p.1396
13. T. Gladman, Proc. Roy. Soc., 1966, Vol.A294, p.298
14. C. Zener, priv. com. to C.S. Smith: Trans. AIME, 1949, vol.175, p.15
15. W.B. Hutchinson, Acta metall., Vol.37, No.4, pp.1047-1056, 1989
16. I.L. Dillamore, Trans. metall. soc. of AIME, 702, Vol.233, april 1965
17. C. Därmann, Proc. ICOTOM 10, Avignon, 1990

Alloys (weight %)						
Identification	Cr	C	N	Ti	Nb	V
A	17	0.06	0.03	0.01	0.01	0.07
B	17	0.02	0.01	0.47	0.01	0.00
C	17	0.02	0.02	0.00	0.64	0.00

Table 2: **Datas for approximate calculation of selective particle drag for alloy B**

a	b	f	γ_{min}	γ_{max}
0.2866 nm	0.2482 nm	$1.9 \cdot 10^{-3}$	0.16 Jm^{-2}	0.5 Jm^{-2}
ρ_o	ρ	K	G	r_{avr}
$\approx 10^{15}$ m^{-2}	$0.28 \cdot 10^{15}$ m^{-2}	0.032 s^{-1}	$81.7 \cdot 10^{9}$ Pa	$0.5 \cdot 10^{-6}$ m

F_R	$F_P(\gamma_{max})$	$F_P(\gamma_{min})$
$7 \cdot 10^5$ Pa	$0.4 \cdot 10^4$ Pa	$0.1 \cdot 10^4$ Pa

a = axis length of bcc cell
b = Burgers vector
f = precipitated volume fraction of particles
γ_{min} = energy of 27° <110> Σ19a grain boundary
γ_{max} = energy of non-special grain boundary
ρ_o = estimated dislocation density after cold rolling
ρ = dislocation density after recovery
K = kinetic constant of recovery
G = Shear modulus
r_{avr} = average particle radius
F_R = driving force of primary recrystallization
F_P = particle drag force

α - fibre : <110> ∥ rolling direction

γ - fibre : <111> ∥ normal direction

η - fibre : <100> ∥ rolling direction

β - fibre : max. ∥ φ_1

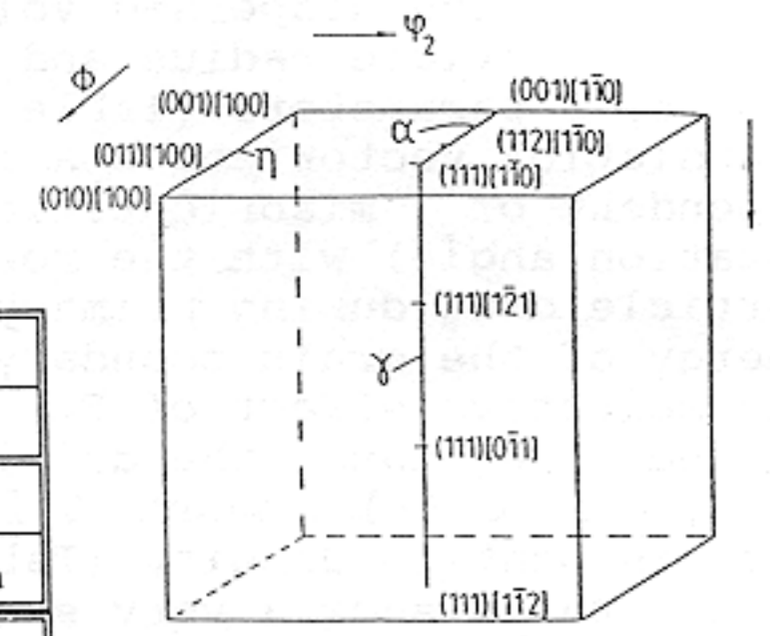

Fig. 1
reduced eulerian space with some important fibres and orientations

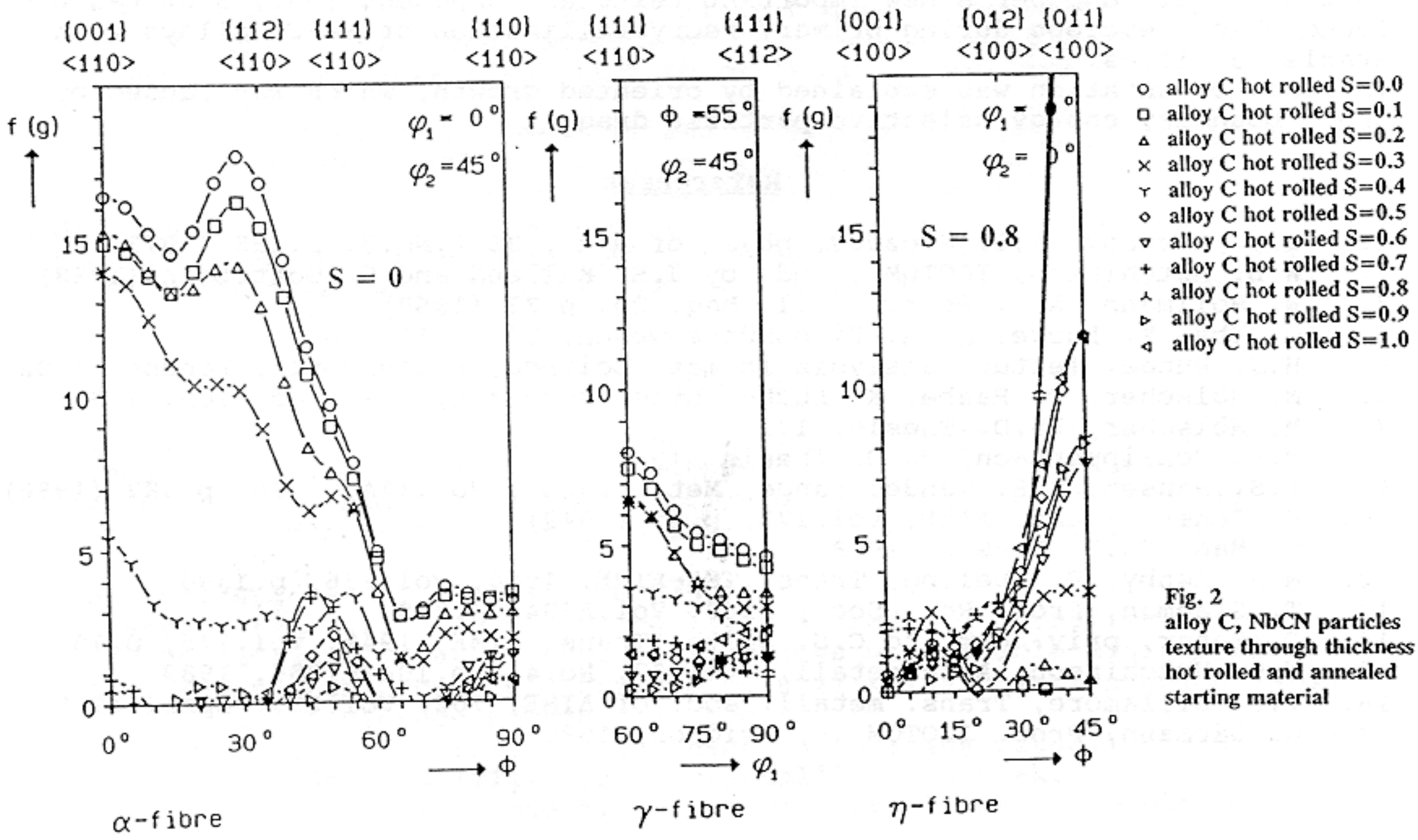

Fig. 2
alloy C, NbCN particles texture through thickness hot rolled and annealed starting material

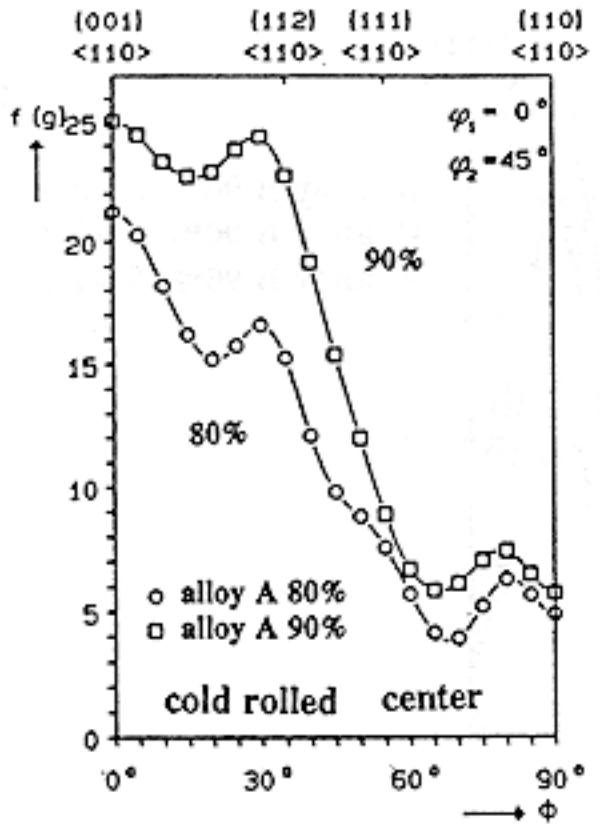

α-fibre

Fig 3a.

Fig. 3a
alloy A, no stable particles
center texture
80% and 90% cold rolled

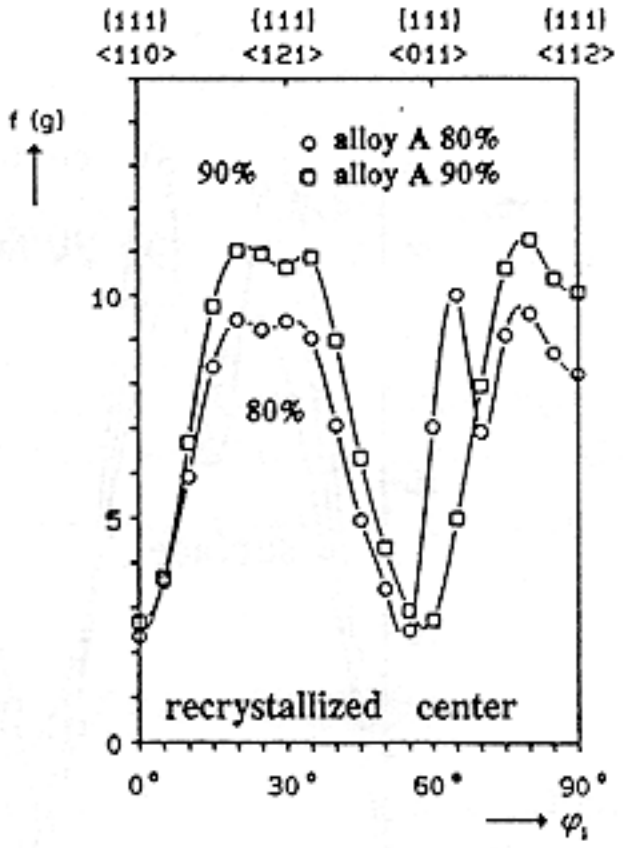

β-fibre (max. density)

Fig 3b.

Fig. 3b
alloy A, no stable particles
center texture
80% and 90% cold rolled
and recrystallized at 1233K

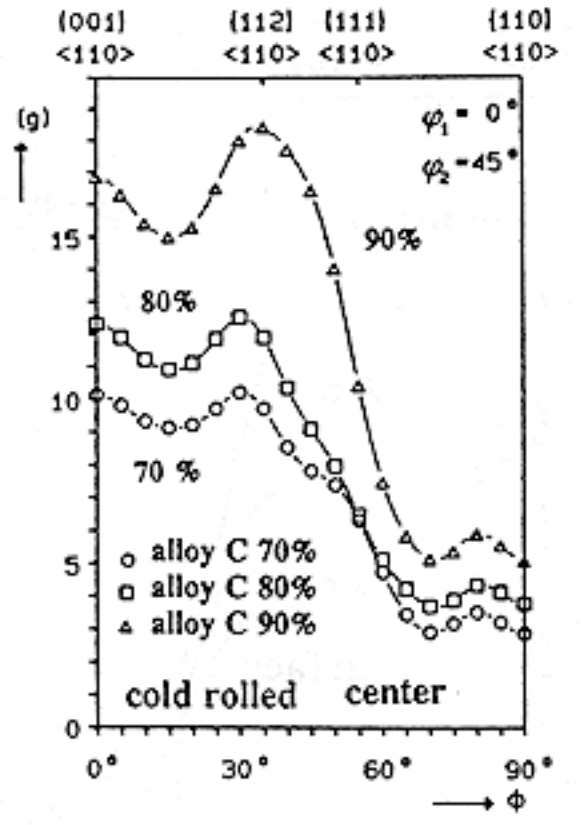

α-fibre

Fig 4a.

Fig. 4a
alloy C, NbCN particles
center texture
70%, 80%, 90% cold rolled

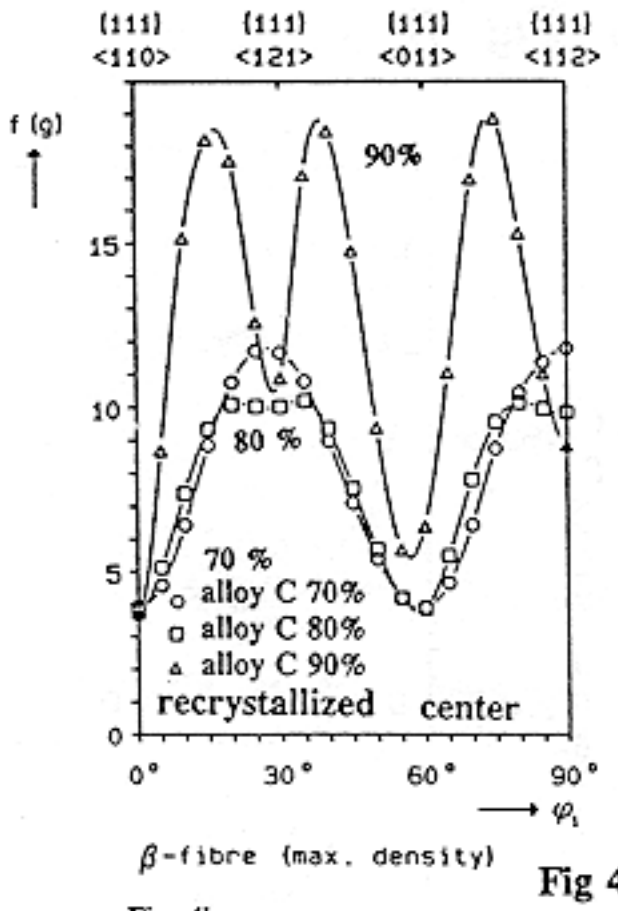

β-fibre (max. density)

Fig 4b.

Fig. 4b
alloy C, NbCN particles
center texture
70%, 80%, 90% cold rolled
and recrystallized at 1233K

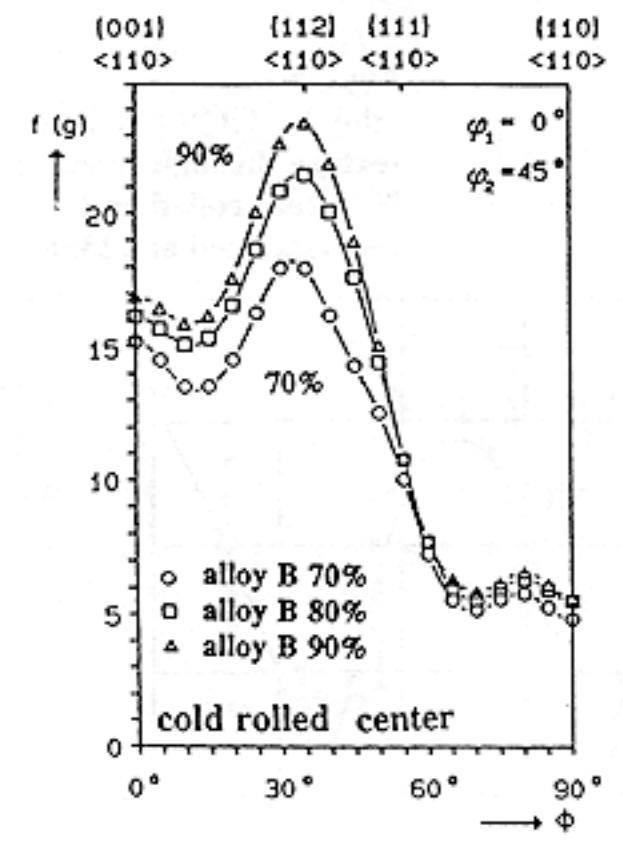

α-fibre

Fig 5a.

Fig. 5a
alloy B, TiCN particles
center texture
70%, 80%, 90% cold rolled

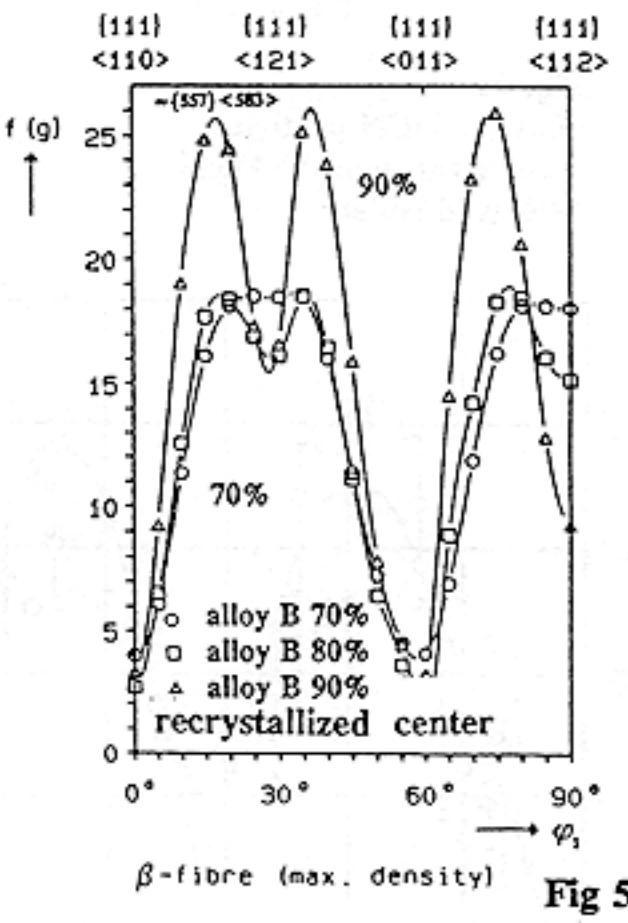

β-fibre (max. density)

Fig 5b.

Fig. 5b
alloy B, TiCN particles
center texture
70%, 80%, 90% cold rolled
and recrystallized at 1233K

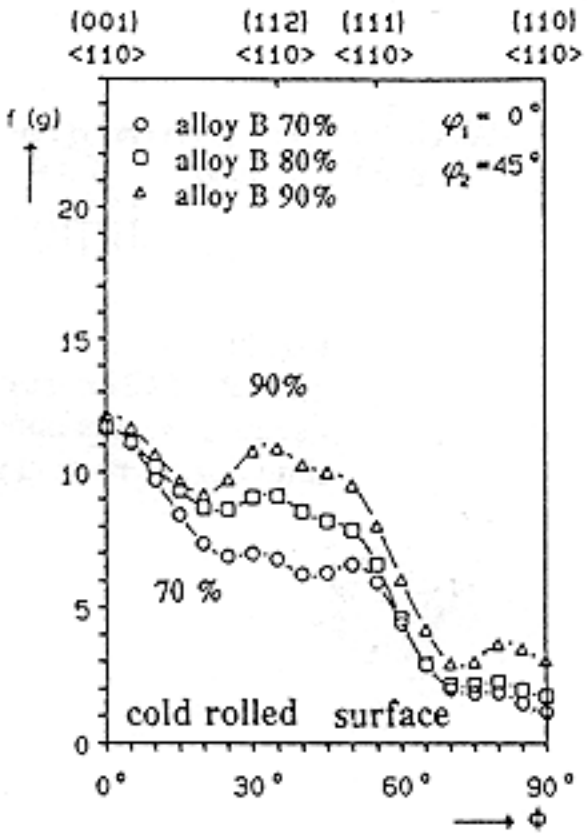

α-fibre

Fig. 6a

Fig. 6a
alloy B, TiCN particles
surface texture
70%, 80%, 90% cold rolled

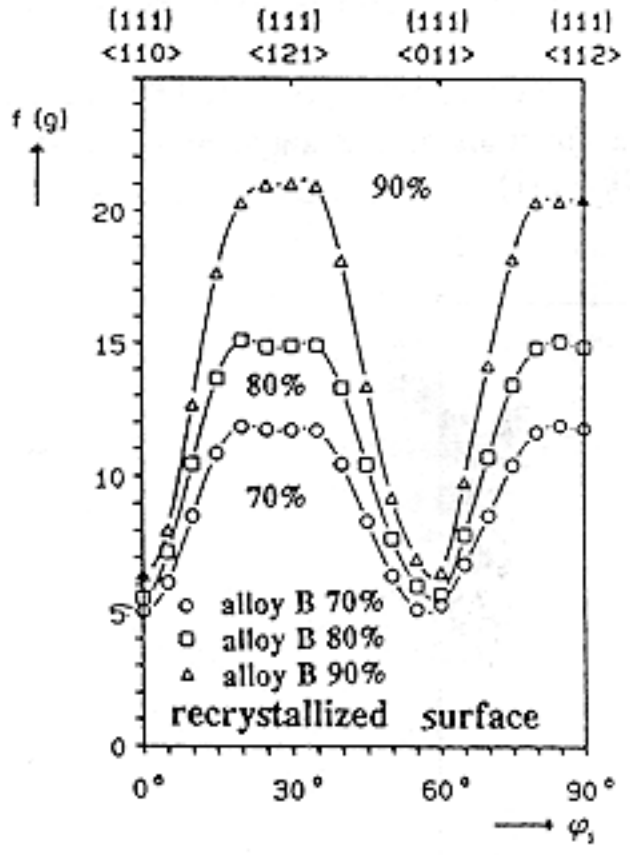

β-fibre (max. density)

Fig. 6b

Fig. 6b
alloy B, TiCN particles
surface texture
70%, 80%, 90% cold rolled
and recrystallized at 1233K

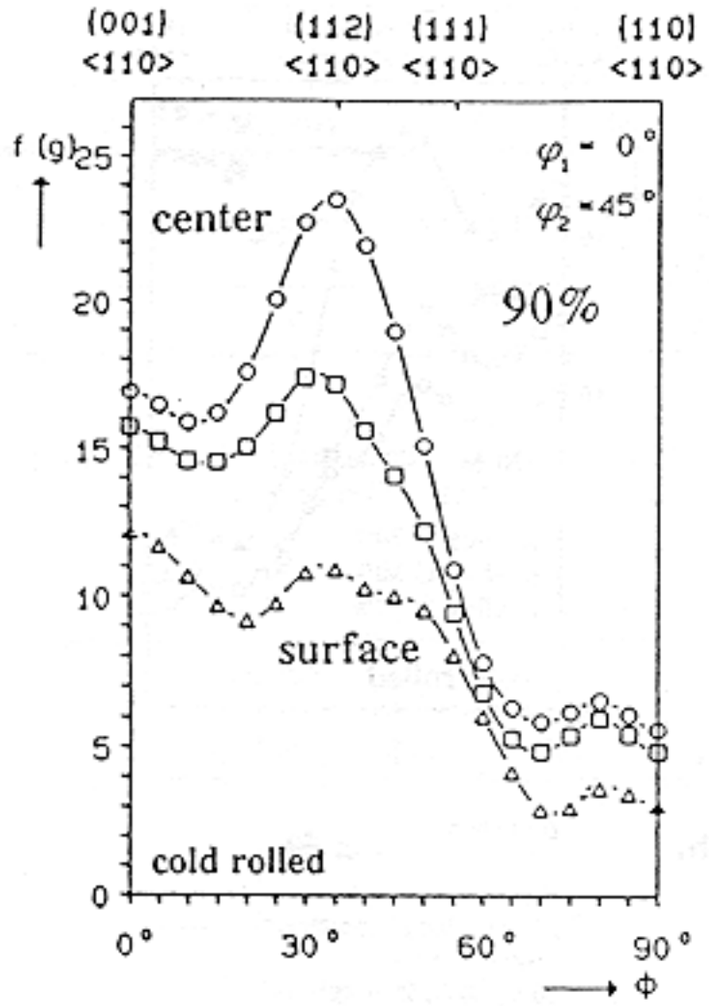

α-fibre

Fig. 7a

Fig. 7a
alloy B, TiCN particles
texture through thickness
90% cold rolled

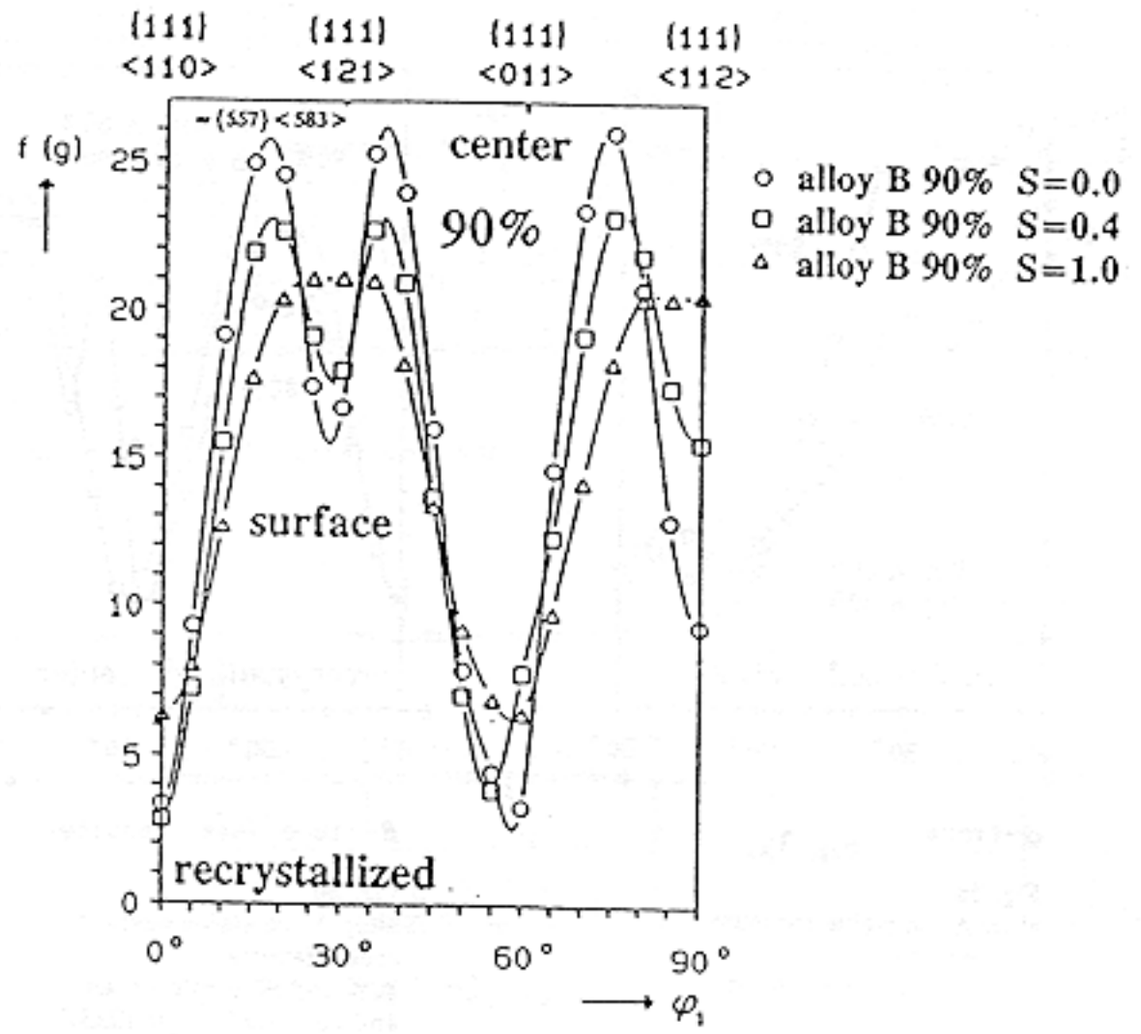

β-fibre (max. density)

Fig. 7b

Fig. 7b
alloy B, TiCN particles
texture through thickness
90% cold rolled and
recrystallized at 1233K

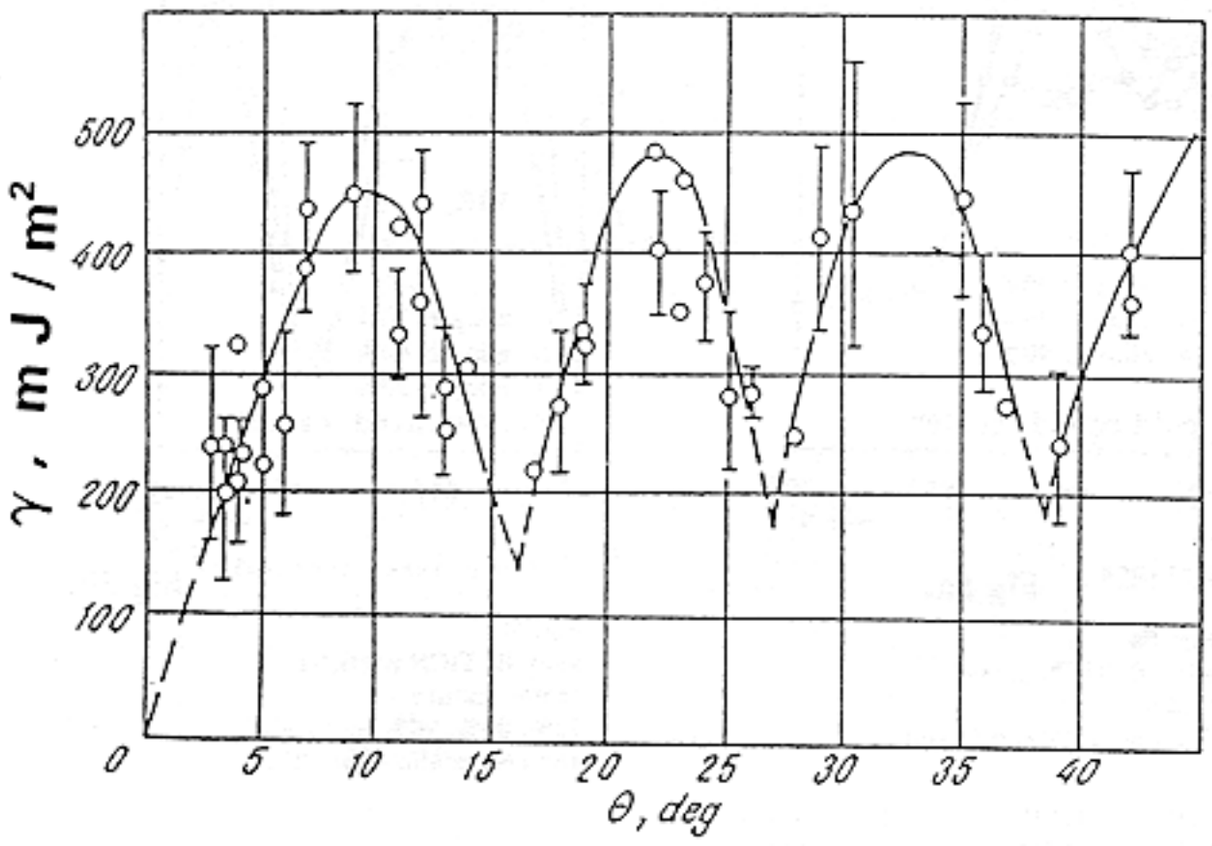

Fig.8
variation in energy of tilt boundaries as a function of the angle of boundary misalignment, rotational axis <110>, (1)

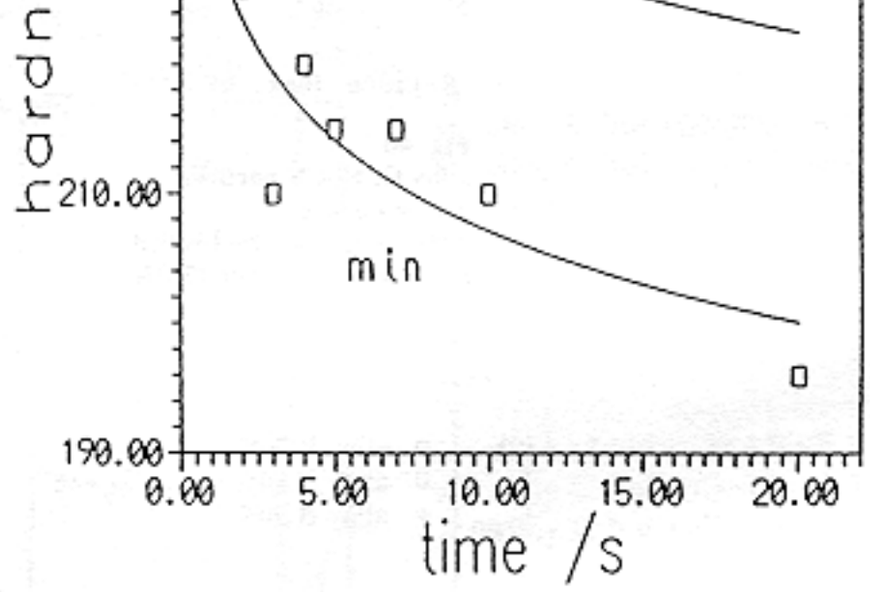

Fig. 9b
alloy B, TiCN particles
hardness versus annealing
time during recovery at 1233K

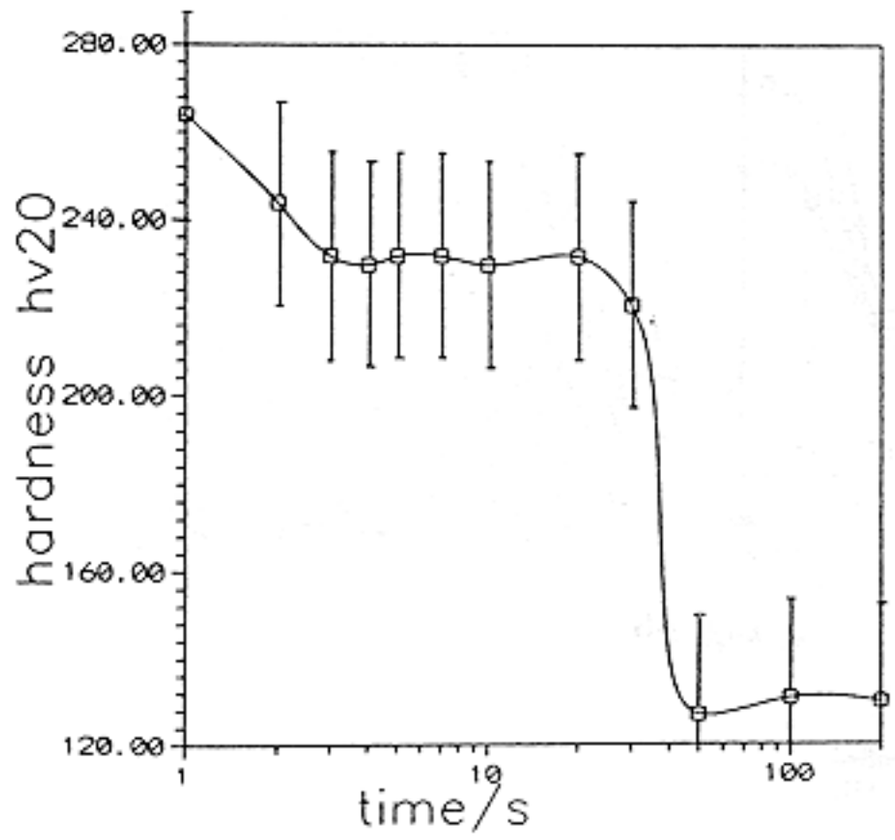

Fig. 9a
alloy B, TiCN particles
hardness versus annealing time
at 1233K after 80% cold rolling